Korean J. Chem. Eng., 36(8), 1313-1320 (2019)
DOI: 10.1007/s11814-019-0308-9

pISSN: 0256-1115
eISSN: 1975-7220

Superhydrophobic and superoleophilic nickel foam for oil/water separation

Kyoung Yong Eum*, Isheunesu Phiri*, Jin Woo Kim, Won San Choi*, Jang Myoun Ko*,†, and Heesoo Jung***,†**

*Department of Applied Chemistry & Biotechnology, Hanbat National University,
125 Dongseo-daero, Yuseong-gu, Daejeon 34152, Korea
**HanKook Tech (#507, Migun Techno World 1) 199, Techno 2-ro, Yuseong-gu, Daejeon 34025, Korea
***Agency for Defense Development (ADD), Yuseong P.O. Box 35-5, Daejeon 34602, Korea
(*Received 13 December 2018 • accepted 25 May 2019*)

Abstract−Superhydrophobic and superoleophilic Ni foam was fabricated by immersion coating and drying method. The Ni foam was immersed in a mixture containing polytetrafluoroethylene (PTFE) and hydrophobic fumed silica (R805). The mixture was dispersed in a poly(vinylidene fluoride) (PVDF) solution and the PVDF was used as a binder. The as-prepared Ni foam showed superhydrophobic and superoleophilic properties simultaneously and had a water contact angle (WCA) of 155° for water and an oil contact angle (OCA) of 0° for oil. The PTFE-coated Ni foam maintained high separation efficiency after repeated separations (40 times) above 96% for the more viscous olive oil/water mixture and above 99% for the hexane/water mixture. The as-prepared nickel foam proved to be an excellent candidate for the separation of oil and water mixtures.

Keywords: Superhydrophobic, Fumed Silica, Nickel Foam, Polytetrafluoroethylene

INTRODUCTION

Oil/water mixture separation has become a growing area of research due the environmental impacts of oil spills, whose effects on the environment are well documented. These mixtures come from various industrial sectors, such as the petroleum, manufacturing, mining, metal fabrication and machining industries, textile and leather processing and rendering industries and also from food processing and restaurants [1]. The oil/water effluents from these industries vary from free oil/water to surfactant-stabilized oil/water emulsions. Emulsions, due to the fine oil particles dispersed in water, are quite difficult, energy intensive and expensive to separate. The large volumes of contaminated mixtures, including from accidents such as the Deepwater Horizon spill in the Gulf of Mexico, obligated the innovation of robust and economical means of separating oil and water mixtures with a high-volume output [1]. One way of separating oil/water mixtures is the use of superoleophilic and superhydrophobic surfaces, which has attracted attention lately [2-5]. After studies on the surface chemistry of the lotus leaf by Barthlott and Neinhuis [6], superhydrophobic materials were fabricated. This was mostly achieved by lowering the surface free energy [7] and or increasing surface coarseness of the solid [8]. Methods for fabricating superhydrophobic surfaces used so far include, but are not limited to, dip coating [9,10], electrospinning [11,12], electrochemical deposition [13,14], electroless deposition [15,16], layer by layer self-assembly [17], chemical etching [18,19], chemical vapor deposition [20-22]. Oil/water separation using superhydrophobic/superoleophilic mesh can be done by a filtration process where only oil passes through the mesh, which is also suitable for separation of large volumes such as industrial effluent [23]. Various surface modifications have been investigated depending on different types of substrates used [24-27]. The separation efficiency depends on a combination of factors such as viscosity of the fluids, pore size, surface tension and rate of fluid flow.

Nickel (Ni) foam has been used lately as a substrate for oil water separation materials because it is a multilayer porous material with low density, high mechanical performance and a high thermal stability. In addition, since Ni foam possesses a multi-linked structure, the superhydrophobic and superoleophilic Ni foam can effectively produce a multi-layer separation for oil/water mixtures, thereby the oil/water separation efficiency of Ni foam should be theoretically higher than that of single-layer metal meshes [16,28,29]. The other advantage of using a metal foam rather than a textile superhydrophobic membrane [30,31] or non-metallic sponge, e.g., polyurethane (PU) sponge is that of weight support. Although the PU sponge has good separation efficiency during continuous flow, it cannot support the weight when the process is scaled-up due to its high flexibility, hence metal foams provide that rigidity which will overcome the weight of the adsorbed oil [32,33]. Gao et al. constructed superhydrophobic and superoleophilic nickel foam for separation of oil/water mixture. The Ni foam was coated with the mixture of $Co(OH)_2$ and Co_3O_4 nanowires and then functionalized with fluoroalkylsilane and produced a water contact angle (WCA) of 156° [16]. Cheng et al. also prepared a device based on nickel foam for the separation of oil/water mixtures to clean up oil spills. The nickel foam was functionalized with silver and 1-dodecanethiol to produce a superhydrophobic and superoleophilic Ni foam [34]. Feng et al. coated a stainless steel mesh with a homogeneous emulsion containing PTFE using a spray-and-dry method. The coated mesh produced a WCA of 156° for water and an oil contact angles (OCA)

†To whom correspondence should be addressed.
E-mail: hsjung@add.re.kr, jmko@hanbat.ac.kr

of 0° for diesel [35]. Ren et al. fabricated a superhydrophobic copper mesh by an immersion process to form $Cu(OH)_2$ nanoneedle arrays. The fabricated copper mesh was folded into a skimming device that had an oil collection efficiency of up to 99.5% [36]. Hu et al. fabricated superhydrophobic nickel foam by spraying the etched nickel foam with a mixed solution containing fluorinated ethylene propylene (FEP), PVDF, ultrafine polyurethane (UPU) and hydrophobic silica nanoparticles ($HSiO_2$) and then calcined at 240 °C. The as-prepared had a water CA of 157° [37]. Many metal surfaces have shown that they adsorbed aerial carbon organic compounds, making these metal surfaces superhydrophobic together with their hierarchical microstructures [38,39].

In this study, PTFE was used because of its low-surface energy [40,41] and the fumed silica (R805) was used to increase roughness of the surface [42,43]. PVDF is a hydrophobic fluorinated polymer with low surface energy, good thermal stability, wear-resistance, chemical inertness and good mechanical properties [42-44]. Previously, PVDF has been used as a membrane and aerogel for oil/water separation [42,45,47], but not as a binder for fabrication of superhydrophobic surfaces to the best of our knowledge. It is also used as a binder in lithium ion battery electrode preparation because of its strong adhesion to metal surfaces [47]; hence, in this study it was used as a binder as well as lowering the surface energy. We hereby report for the first time the use of PVDF as a binder for a mixture of PTFE and fumed silica on a metal surface by simple immersion coating and drying method to from a superhydrophobic nickel foam. The Ni foam was coated using a homogeneous mixture of PTFE and R805 in a PVDF solution. This composite coating is designed to reduce surface energy and to improve the surface roughness, which are the two important factors of achieving superhydrophobic surfaces [43]. This method of coating was used because it is simple and fast and avoids the use of expensive reagents like fluoroalkylsilanes. The coated nickel foam coactively enables a fluorine-covered surface to be fashioned and provides a rigid metallic frame that traps the composite material in its spaces, thereby enhancing the superhydrophobicity.

EXPERIMENTAL

1. Materials

PVDF in powder form (MW=534,000), PTFE (FW=100.0) in powder form, modified AEROSIL fumed silica (R805) and nickel form (volume density: 0.32 gcm^{-3}, thickness 1.35 mm, average pore diameter: 130 μm, pore number: 110 PPI) were purchased from Sigma Aldrich. Sodium chloride (99.0%), potassium hydroxide (Min. 85.0%), hydrochloric acid (35.0-37.0%), hexane (Min. 95.0%) and dimethyl sulfoxide (DMSO) (Min. 99.6%) were purchased from Duksan Reagents, Olitalia extra virgin Olive oil and soy bean oil were obtained from a local market. All chemicals were used as received without any further purification. The deionized water was produced using an AquaMax-Ultra deionizer.

2. Preparation of Coating Mixture

A mixture containing 60 wt% PTFE, 20 wt% R805, 20 wt% PVDF (binder, 8 wt% dissolved in DMSO) was ball milled for 30 mins (MSG-D500 ball mill at 1,000 rpm using zirconium balls of 2 mm diameter) to produce a slurry which was used for coating of the Ni foam.

3. Preparation of PTFE-coated Nickel Foam

A piece measuring 4 cm×4 cm of Ni foam was ultrasonically cleaned in acetone for 10 mins to remove any grease and then again ultrasonically etched in 1 M HCl for a further 10 mins to remove any oxide layer. The Ni foam was then dried first using compressed air for 30 seconds and then oven dried at 100 °C for 15 mins. About 20 mL of the slurry was poured into a petri dish (85 mm diameter, 10 mm height). The cleaned Ni foam was immersed in the slurry for 1 min and immediately dried in an oven at 115 °C for 120 mins to remove all the DMSO solvent. The immersion process was repeated three times to obtain a relatively even coating on the mesh. A summary of the process and photographs are shown in Fig. 1.

4. Preparation of Oil/Water Mixtures

The oil/water mixtures were prepared by mixing 20 mL of oil and 20 mL of water (1 : 1 v/v % oil/water). Different oil/water mixtures were prepared using different oils, i.e., hexane, soybean oil and olive oil.

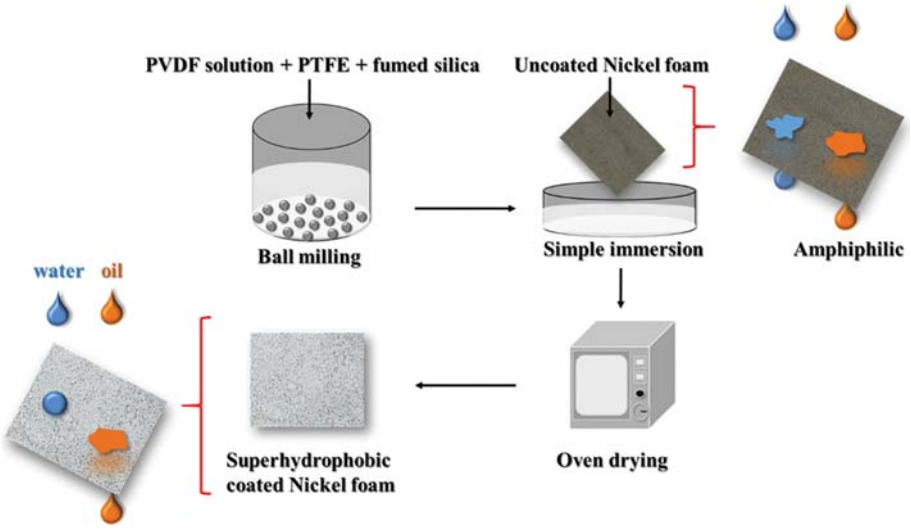

Fig. 1. Schematic diagram of the coating process.

5. Oil/Water Separation Experiment

The coated Ni foam was fixed between two glass tubes of diameter 20 mm (effective area of Ni foam, A_{eff}=3.14×10^{-4} m^2). The separation process was achieved by gravity at an angle to allow the oil phase to be in contact with the foam for separation since oil is less dense than water. The separation efficiency was calculated as the ratio of the residual volume to the initial volume in the mixtures when there was no more dripping of oil seen from the filter and calculated using Eq. (1) [48].

$$\eta = \frac{V_1}{V_0} \times 100 \quad (1)$$

where V_1 is the volume of oil after separation and V_0 is the initial volume of oil before separation. Flux (F) measurements, under a fixed gravity pressure were done for the oils afore mentioned, and calculated using Eq. (2).

$$F = \frac{\Delta V}{\Delta t \cdot A_{eff}} \quad (2)$$

where ΔV (L) is change in volume (in liters), Δt (h) is change in time (in hours) and A_{eff} (m^2) is the effective area (in square meters) of the coated Ni foam. The intrusion pressure (ΔP), which indicates the maximum weight of the water the coated Ni foam can support, was calculated using Eq. (3) [49]:

$$\Delta P = \rho g h_{max} \quad (3)$$

where ρ is the density of the water, g is acceleration of gravity, and h is the maximum height of water a coated nickel foam can support.

6. Instruments and Characterization

The contact angle, work of adhesion, wetting energy, and spread-

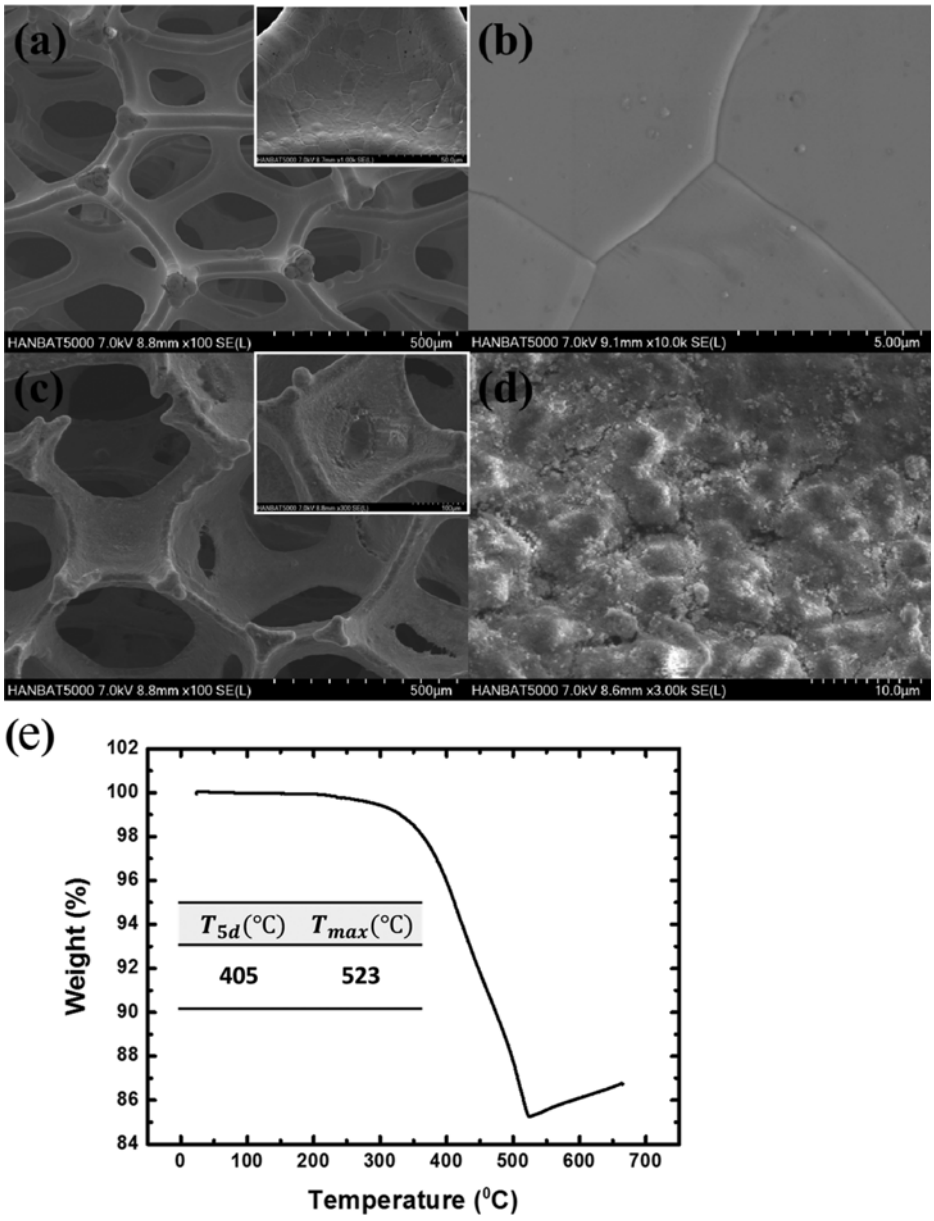

Fig. 2. FE-SEM images of (a), (b) the bare Ni foam and (c), (d) coated Ni foam. (e) TGA analysis for the coated Ni foam.

ing coefficient were determined using an SEO Phoenix 300 touch contact angle analyzer. The as-prepared Ni foam was observed using a field emission scanning electron microscope (Thermal type FE-SEM, Hitachi S-5000) and digital images were taken with a Lumix DMC lx10 camera.

RESULTS AND DISCUSSION

1. Structure of the PTFE-coated Ni Foam

The FE-SEM images of the bare Ni foam are in Figs. 2(a) and (b), and the coated Ni foam are in Figs. 2(c) and (d). The bare Ni foam possesses a multilayer porous and interlinked three-dimensional (3D) structure similar to a sponge and the skeletons of bare Ni foam are relatively smooth. The pore sizes of the bare Ni foam non-uniformly ranged from 250 to 450 μm. After the coating, the smooth skeletons were covered with the coating, creating a rough surface (Fig. 2(d)), and the pores were also to some degree filled with the coating material with a rough surface (Fig. 2(c)). These results indicated that the as-prepared Ni foam had a rough surface and micro spaces.

The TGA results are shown in Fig. 2(e). The coated Ni foam show thermal stability for temperatures below 250 °C with a T_{5d} (temperature at 5% weight loss) of 405 °C and a T_{max} of 523 °C. The hydrocarbon chain of the R805 and the PTFE are combusted-off, which explains the loss in weight at higher temperatures. After T_{max}, the percentage weight starts to rise again due to the formation of nickel oxide of the surface of the nickel foam since the TGA analysis was done in air.

2. Surface Properties of PTFE-coated Ni Foam Towards Oil/water

Before coating, the nickel foam was amphiphilic as shown in Fig. 3(f). The OCA using coated material was 0° for both hexane and olive oil. The WCAs for the different aqueous solutions were 155°, 153°, 152° and 152° for pure water, 1 M HCl, 1 M KOH and 1 M NaCl,, respectively, as shown in Fig. 3(a)-(d). Table 1 shows the wetting properties of the coated Ni foam towards different liquids. The wetting energy, spreading coefficient and work of adhesion for the oils were above 72, –0.76, and 144 mNm^{-1}, respectively (Table 1). Also, the wetting energy, spreading coefficient and work of adhesion for the aqueous solutions recorded lowest figures with pure water, −48, −121 and 24 mNm^{-1}, showing that the coated Ni foam possess super-low water affinity, hence are superhydrophobic [50]. It was observed that oil quickly spread and permeated the foam, while the water droplets stayed spheroidal on the surface of the coated foam as shown in Fig. 3(e). PTFE improved the hydrophobicity because it is a typically low-surface energy material (20 mNm^{-1}) [41]. The hydrophobic silica forms aggregates due to the formation of hydrogen bonds between the fumed silica particles via the silanol groups on their surfaces [51,52]. These aggregates have

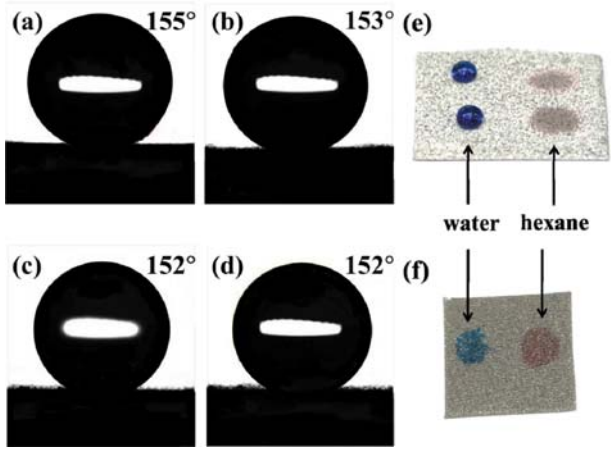

Fig. 3. Contact angle images of (a) deionized water, (b) 1 M HCl, (c) 1 M KOH, (d) 1 M NaCl (Drop volume was 21.58 μL). Wettability tests with water and hexane for (e) coated Ni foam (f) bare Ni foam.

strong adhesion to PTFE and PVDF caused by the van der Waal forces of attraction due to the presence of the hydrophobic chains ($-C_8H_{17}$) in the R805 and the ($-CF_2-$) group in the PTFE and PVDF, thereby enhancing the superhydrophobicity [43,53]. This exhibited super-high oil affinity thus superoleophilicity of the coated Ni foam. The superoleophilic properties of the coated Ni foam can be explained by the Wenzel equation [54] as follows:

$$\cos\theta_c = r\cos\theta_0 \quad (4)$$

where θ_c is the apparent WCA of a rough substrate, θ_0 represents the WCA of a native flat surface, and r is the surface roughness factor. The θ_0 in our experiment was 113°. The Wenzel equation shows that by increasing surface roughness and low surface energy of the coated nickel foam, the oleophilicity of the foam can be enhanced.

The Cassie model can be used to explain the superhydrophobicity of the nickel foam. Due to the roughness and the low surface energy of the surface, water droplets cannot infiltrate into the rough surface such that air is trapped between water and foam, forming a layer of air making the mesh superhydrophobic. The Cassie equation [55] can be expressed as:

$$\cos\theta_c = f_s\cos\theta_0 + f_s - 1 \quad (5)$$

where θ_c is the WCA (155°), θ_0 is the WCA of the flat surface (113°), and f_s is the area fraction on the surface. Thus, when f_s decreases for a larger roughness surface, the WCA increases. The coated nickel foam had a rough surface and a large WCA, which indicates a relative small area fraction. These observations show us that the coating made the nickel form superoleophilic and superhydrophobic.

The Gibbs energy (ΔG) also explains the superhydrophobicity of

Table 1. Wetting properties of the PTFE coated Ni foam

Property	Water	HCl	KOH	NaCl	Hexane	Olive oil
Wetting energy [mNm^{-1}]	−48.32	−44.38	−41.39	−41.57	76.79	72.04
Spreading coefficient [mNm^{-1}]	−121.12	−117.18	−114.19	−114.37	−0.69	−0.76
Work of adhesion [mNm^{-1}]	24.48	28.42	31.41	31.23	148.15	144.84

the coated nickel foam. For the spreading process, a Gibbs energy equation is derived,

From Young's equation:

$$\gamma^s=\gamma^{ls}+\gamma^l\cos\theta \quad (6)$$

And the Gibbs equation:

$$\Delta G=\gamma^{ls}+\gamma^l-\gamma^s \quad (7)$$

Another Gibbs equation is derived as follows:

$$\Delta G=-\gamma^l(\cos\theta-1) \quad (8)$$

where γ is the surface tension; s and l are solid and liquid phases, and θ is the WCA. For a superhydrophobic surface, the WCA≥150°, then ΔG>0, which implies that water droplets will not spread spontaneously on the surface. Furthermore, when θ increases, ΔG also increases, making it more difficult for water droplets to spread. Contrariwise, the OCA is 0°; as a result, the ΔG is 0, implying that the surfaces can be easily wetted by oil [43,56].

Fig. 4 shows the contact angles after treatment in concentrated solutions: 10 M H_2SO_4, 10 M NaOH, saturated Na_2SO_4 and water as a control. The contact angle in the treatment with water changed slightly from 153° to 152° leaving the foam still superhydrophobic. However, treatments with highly acidic, alkaline and salt solution resulted in the foam changing from superhydrophobic to hydrophobic, which we attributed to corrosion.

3. Oil/Water Separation

The oil/water separation experiment was performed using a simple separation device as shown in Fig. 5(a). Fig. 5(b) shows that water does not pass through the coated Ni foam, and Fig. 5(c) shows that hexane can pass through the coated Ni foam. Upon pouring the mixture of hexane and water, the hexane quickly permeates through the coated foam but the water remains trapped in the upper glass tube as shown in Fig. 5(g), same as for soybean oil and olive oil Figs. 5(h) and (i), respectively. However, as the density and the viscosity of the oil increased, the rate of it passing through the foam decreased as expected in Figs. 5(h) and (i).

The coated nickel foam had a separation efficiency of 99.8% for the water/hexane mixture, 98.9% for the water/soy oil mixture and 97.2% for the olive oil as shown in Fig. 6(a). The olive oil was the most viscous of all the oils investigated. Some of the olive oil remained adsorbed on the coated foam, thereby reducing efficiency to just below 98%. Repeated separations performed showed that the separation efficiency reduced slightly after 50 cycles as shown in Fig. 6(b). Repeated cycles were done to test the stability of the coated nickel foam. After 40 cycles, the WCAs changed from 155° (superhydrophobic) to 143° (hydrophobic) as shown in Fig. 6(d). The foam also maintained a high separation efficiency above 97% for the different oil/water mixtures, showing the good stability of

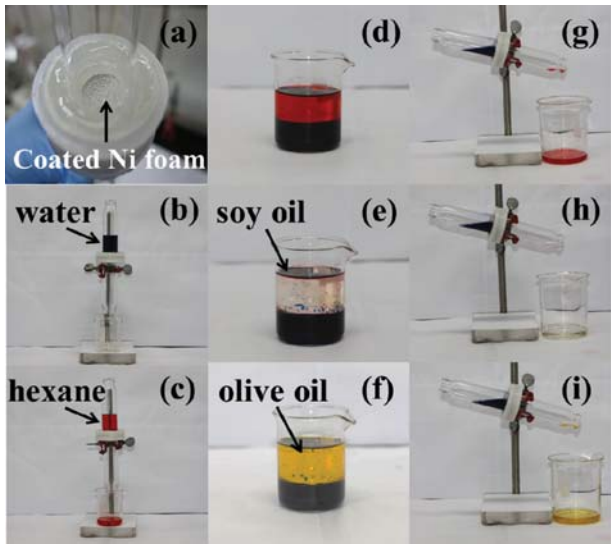

Fig. 5. (a) The coated Ni foam was fixed between two glass tubes, (b) water suspended at the upper tube, (c) hexane passing through the coated foam. The oil and water mixtures (d) hexane and water (e) soy oil and water (f) olive oil and water. The separation of oil and water mixtures with (d) hexane/water, (e) soybean oil/water, and (f) olive oil/water.

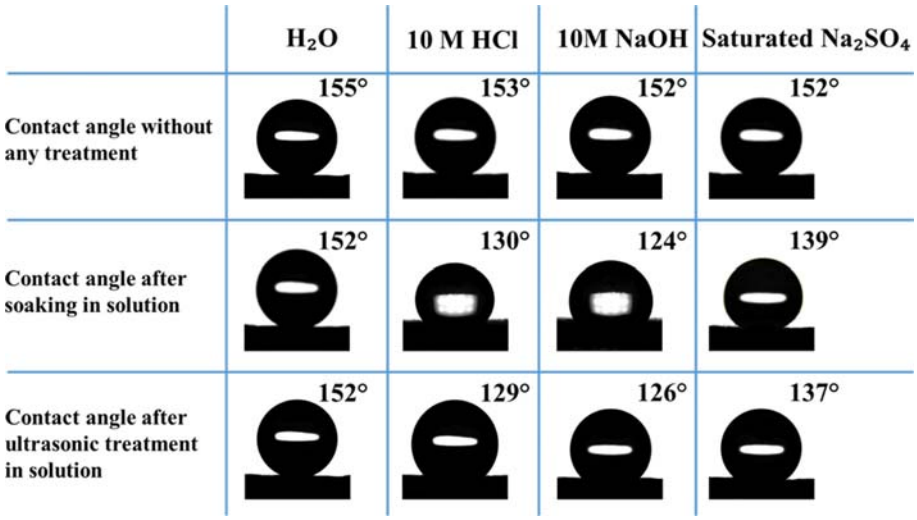

Fig. 4. Contact angles of the coated nickel foam after soaking in the respective solutions for 14 days and other samples ultrasonicated in the solutions for 1 hour.

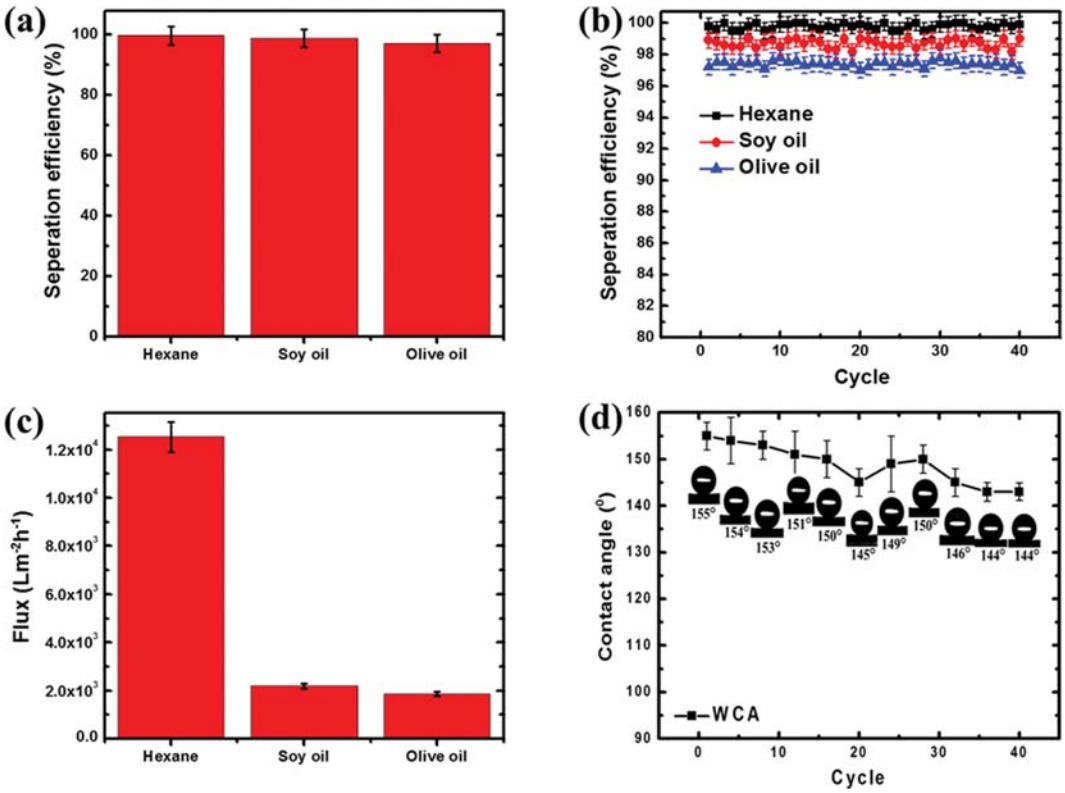

Fig. 6. (a) The separation efficiency of the coated Ni foams for a selection of oil and water. (b) Effect of cycle times on the separation efficiency and WCAs of the coated Ni foams. (c) Flux for the coated Ni foam for different oils. (d) Change in WCA with increased cycling.

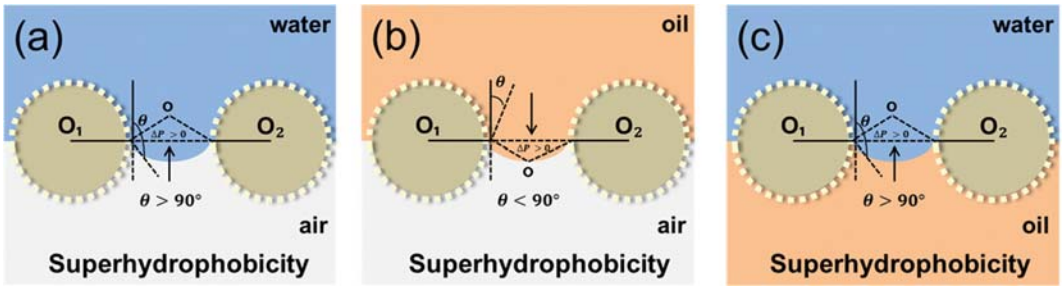

Fig. 7. Schematic diagrams of the liquid wetting model on the coated nickel foam (a) in air, the foam exhibits superhydrophobicity because ΔP>0; thus, water cannot permeate through the foam. (b) In air, the foam shows superoleophilicity, which allows oil to permeate the foam and cannot withstand pressure because ΔP<0. (c) After oil permeation, some oil can be trapped among the interspaces between the PTFE, R805 and PVDF molecules, hence the mesh displays superhydrophobicity, and the mesh can withstand the water, because ΔP>0. O is the center of the spherical of the meniscus; O_1 and O_2 are the cross-section center of the foam.

coatings indicating that this superhydrophobic foam is a good candidate in oil-polluted water treatments [57].

Flux decreased with an increase in oil viscosity, as expected, which agrees with the inverse proportional relation between flux and kinetic viscosity [58] with hexane having a very high flux of 12,525 $Lm^{-2}h^{-1}$ that is 63-times higher than the commercial filtration membranes (20-200 $Lm^{-2}h^{-1}$) [59] and soy oil with a flux of 2,191 $Lm^{-2}h^{-1}$ and lastly olive oil having the lowest flux of 1,860 $Lm^{-2}h^{-1}$. Fig. 6(c) shows the graph for flux. The high flux is due to the superhydrophobicity and superoleophilicity of the coated foam as well as the high porosity of the foam.

Fig. 7 shows the model for the wetting processes on the coated nickel foam. Generally, the pore bottom can be wetted if the intrusion pressure (ΔP) is exceeded, which is explained as follows:

$$\Delta P = -\frac{2\gamma}{R} = -\frac{l\gamma\cos\theta_A}{A} \quad (9)$$

where γ is the surface tension, R is the meniscus's radius, l is the pore's perimeter, θ_A is the advancing contact angle on the foam, and A is the pore's area [60,61]. From Eq. (6), if θ_A>90°, there will be no intrusion to some degree because ΔP>0. The WCA was >150° for different pH aqueous solutions for the coated nickel foam as shown in Fig. 3; thus, the coated foam was superhydrophobic and the water could not pass through the coated foam as shown in Fig.

4(b). The oil contact angle (OCA) was almost 0°, which means that $\Delta P<0$, showing that the oil can pass through the foam quickly as shown in Fig. 4(c). As the oil permeates through the pores, some of it is trapped (but small enough not to cause clogging of the foam) because of the superoleophilicity of the coated foam, thereby enhancing the superhydrophobicity and a high WCA on the coated nickel foam [48,62]. The ΔP was calculated using Eq. (3) and it was about 7.8 kPa, which entails that water cannot permeate the coated foam below this intrusion pressure.

CONCLUSION

We prepared a substrate with both superhydrophobic and superoleophilic properties by coating Ni foam with a coating material of PTFE powder and fumed silica dispersed in a PVDF solution that acted as a binder. The separation of different oil/water mixtures was quite efficient in terms of separation efficiency compared to other methods for separation of oil/water. It also had a high selectivity and an easy production process, thus making the as-prepared Ni foam suitable for many practical applications. The coating material composition and the production technology can be scaled-up to provide functional separation and filtration equipment suitable for large-scale oil/water separation.

ACKNOWLEDGEMENTS

This project was supported by the Civil-Military Technology Cooperation Program and Agency for Defense Development of Korea.

SUPPORTING INFORMATION

Additional information as noted in the text. This information is available via the Internet at http://www.springer.com/chemistry/journal/11814.

REFERENCES

1. G. Kwon, E. Post and A. Tuteja, *MRS Communications*, **5**, 475 (2015).
2. A. S. K. Kumar, S. S. Kakan and N. Rajesh, *Chem. Eng. J.*, **230**, 328 (2013).
3. Q. Zhu, Q. Pan and F. Liu, *J. Phys. Chem. C*, **115**, 17464 (2011).
4. C. Wang, T. Yao, J. Wu, C. Ma, Z. Fan, Z. Wang, Y. Cheng and Q. L. Yang, *ACS Appl. Mater. Interfaces*, **1**, 2613 (2009).
5. C. Huei, N. Johnson, J. Drelich and Y. K. Yap, *Carbon*, **49**, 669 (2010).
6. W. Barthlott, C. Neinhuis, H. Verlot and C. L. Schott, *Planta*, **202**, 1 (1997).
7. A. Nakajima, K. Abe, K. Hashimoto and T. Watanabe, *Thin Solid Films*, **376**, 4 (2000).
8. T. Ishizaki, J. Hieda, N. Saito, N. Saito and O. Takai, *Electrochim. Acta*, **55**, 7094 (2010).
9. J. Song, Y. Lu, J. Luo, S. Huang, L. Wang, W. Xu and I. P. Parkin, *Adv. Mater. Interfaces*, **2**, 1500350 (2015).
10. Q. Zhu, Y. Chu, Z. Wang, N. Chen, L. Lin, F. Liu and Q. Pan, *J. Mater. Chem. A*, **1**, 5386 (2013).
11. R. Menini and M. Farzaneh, *Polym. Int.*, **57**, 77 (2008).
12. J. Wu, N. Wang, L. Wang, H. Dong, Y. Zhao and L. Jiang, *ACS Appl. Mater. Interfaces*, **4**, 3207 (2012).
13. Wu and G. Shi, *J. Phys. Chem. B*, **110**, 11247 (2006).
14. S. Santhanagopalan, F. Teng and D. D. Meng, *Langmuir*, **27**, 561 (2011).
15. Z. She, Q. Li, Z. Wang, L. Li, F. Chen and J. Zhou, *ACS Appl. Mater. Interfaces*, **4**, 4348 (2012).
16. Z. Gao, Q. Liu, J. Wang, J. Liu, W. Yang, Z. Gao and L. Liu, *Appl. Surf. Sci.*, **289**, 417 (2013).
17. S. Nishimoto, H. Sekine, H. Zhang, Z. Liu, K. Nakata, T. Murakami, Y. Koide and A. Fujishima, *Langmuir*, **25**, 7226 (2009).
18. Z. J. Chen, Y. B. Guo and S. M. Fang, *Surf. Interface Anal.*, **42**, 1 (2010).
19. L. Li, V. Breedveld and W. D. Hess, *ACS Appl. Mater. Interfaces*, **4**, 4549 (2012).
20. A. Borras, A. Barranco and A. R. Gonzalez-Elipe, *Langmuir*, **24**, 8021 (2008).
21. C. F. Wang, F. S. Tzeng, H. G. Chen and C. J. Chang, *Langmuir*, **28**, 10015 (2012).
22. X. Ding, S. Zhou, G. Gu and L. Wu, *J. Mater. Chem.*, **21**, 6161 (2011).
23. X. Chen and W. Shen, *Chem. Eng. J.*, **308**, 18 (2017).
24. L. Wu, J. Zhang, B. Li and A. Wang, *J. Colloid Interface Sci.*, **413**, 112 (2014).
25. L. Feng, Z. Zhang, Z. Mai, Y. Ma, B. Liu, L. Jiang and D. Zhu, *ACS Appl. Mater. Interfaces*, **5**, 3 (2013).
26. S. Li, J. Huang, Z. Chen, G. Chen and Y. Lai, *J. Mater. Chem. A*, **5**, 31 (2017).
27. M. Ge, C. Cao, J. Huang, X. Zhang, Y. Tang, X. Zhou, K. Zhang, Z. Chen and Y. Lai, *Nanoscale Horiz.*, **3**, 235 (2018).
28. D. Cao, Y. Gao, G. Wang, R. Miao and Y. Liu, *Int. J. Hydrogen Energy*, **35**, 807 (2010).
29. E. B. V All, *Appl. Surf. Sci.*, **254**, 6002 (2008).
30. X. Zhua, Z. Zhang, Y. Songa, J. Yana, Y. Wanga and G. Rena, *J. Taiwan Inst. Chem. Eng.*, **71**, 421 (2017).
31. X. Dong, S. Gao, J. Huang, S. Li, T. Zhu, Y. Cheng, Y. Zhao, Z. Chen and Y. Lai, *J. Mater. Chem. A*, **7**, 2122 (2019).
32. M. W. Lee, S. An, S. S. Latthe, C. Lee, S. Hong and S. S. Yoon, *ACS Appl. Mater. Interfaces*, **5**, 10597 (2013).
33. B. Wang, W. Liang, Z. Guo and W. Liu, *Chem. Soc. Rev.*, **44**, 336 (2015).
34. M. Cheng, Y. Gao, X. Guo, Z. Shi, J. Chen and F. Shi, *Langmuir*, **27**, 7371 (2011).
35. L. Feng, Z. Zhang, Z. Mai, Y. Ma, B. Liu, L. Jiang and D. Zhu, *Angew. Chem.*, **116**, 2046 (2004).
36. G. Ren, Y. Song, X. Li, Y. Zhou, Z. Zhang and X. Zhu, *Appl. Surf. Sci.*, **428**, 520 (2018).
37. Y. Hu, Y. Zhu, H. Wang, C. Wang, H. Li, X. Zhang, R. Yuan and Y. Zhao, *Chem. Eng. J.*, **322**, 157 (2017).
38. L. B. Boinovich, A. M. Emelyanenko, A. S. Pashinin, C. H. Lee, J. Drelich and Y. K. Yap, *Langmuir*, **28**, 1206 (2012).
39. T. Smith, *J. Colloid Interface Sci.*, **75**, 51 (1980).
40. F. Wang, S. Lei, Y. Xu and J. Ou, *Chem. Phys. Chem.*, **16**, 2237 (2015).
41. L. Feng, Z. Y. Zhang, Z. H. Mai, Y. M. Ma, B. Q. Liu, L. Jiang and

D. B. Zhu, *Angew. Chem.*, **116**, 2046 (2004).
42. J. Gao, X. Huang, H. Xue, L. Tang and R. K. Y. Li, *Chem. Eng. J.*, **326**, 443 (2017).
43. L. Peng, W. Lei, P. Yu and Y. Luo, *RSC Adv.*, **6**, 10365 (2016).
44. Y. Yu, H. Chen, Y. Liu, V. S. J. Craig, L. H. Li, Y. Chen and A. Tricoli, *Polymer*, **55**, 5616 (2014).
45. Y. Zhu, W. Xie, F. Zhang, T. Xing and J. Jin, *ACS Appl. Mater. Interfaces*, **9**, 9603 (2017).
46. M. Obaid, H. O. Mohamed, A. S. Yasin, M. A. Yassin, O. A. Fadali, H. Y. Kim and N. A. M. Barakat, *Water Res.*, **123**, 524 (2017).
47. M. A. Spreafico, P. Cojocaru, L. Magagnin, F. Triulzi and M. Apostolo, *Ind. Eng. Chem. Res.*, **53**, 9094 (2014).
48. W. Ma, Z. Guo, J. Zhao, Q. Yu, F.Wang, J. Han, H. Pan, J. Yao, Q. Zhang, S. K. Samal, S. C. De Smedta and C. Huanga, *Sep. Purif. Technol.*, **177**, 71 (2017).
49. W. Ma, Q. Zhang, S. K. Samal, F. Wang, B. Gao, H. Pan, H. Xu, J. Yao, X. Zhan, S. C. De Smedt and C. Huang, *RSC Adv.*, **6**, 41861 (2016).
50. Y. Xiu, L. Zhu, D. W. Hess and C. P. Wong, *J. Phys. Chem*, **112**, 11403 (2008).
51. T. Nazir, A. Afzal, H. M. Siddiqi, Z. Ahmad and M. Dumon, *Prog. Org. Coat.*, **69**, 100 (2010).
52. F. Ardeshiri, A. Akbari, M. Peyravi and M. Jahanshahi, *Korean J. Chem. Eng.*, **36**, 255 (2019).
53. W. A. Zisman, *ACS Adv. Chem.*: Washington, DC, **43**, 1 (1964).
54. R. N. Wenzel, *Ind. Eng. Chem.*, **28**, 988 (1936).
55. J. Drelich, J. D. Miller, A. Kumar and G. M. Whitesides, *Colloids Surfaces A: Physicochem. Eng. Aspects*, **93**, 1 (1994).
56. L. Peng, S. Yuan, G. Yan, P. Yu and Y. Luo, *J. Appl. Polym. Sci.*, **131**, 40886 (2014).
57. Z. Li, T. Shi, T. Zhang, Q. Guo, F. Qiu, X. Yue and D. Yang, *Korean J. Chem. Eng.*, **36**, 92 (2019).
58. J. Li, G. Zhang, Y. Yao, Z. Jing, L. Zhou and Z. Ma, *RSC Adv.*, **6**, 60094 (2016).
59. B. Chakrabarty, A. K. Ghoshal and M. K. Purkait, *J. Membr. Sci.*, **325**, 427 (2008).
60. J. P. Youngblood and T. J. Mccarthy, *Macromol.*, **32**, 6800 (1999).
61. B. Liu and F. F. Lange, *J. Colloid Interface Sci.*, **298**, 899 (2006).
62. I. Phiri, K. Y. Eum, J. W. Kim, W. S. Choi, J. M. Ko and H. Jung, *J. Ind. Eng. Chem.*, **73**, 78 (2019).

Supporting Information

Superhydrophobic and superoleophilic nickel foam for oil/water separation

Kyoung Yong Eum*, Isheunesu Phiri*, Jin Woo Kim, Won San Choi*, Jang Myoun Ko*,†, and Heesoo Jung***,†**

*Department of Applied Chemistry & Biotechnology, Hanbat National University,
125 Dongseo-daero, Yuseong-gu, Daejeon 34152, Korea
**HanKook Tech (#507, Migun Techno World 1) 199, Techno 2-ro, Yuseong-gu, Daejeon 34025, Korea
***Agency for Defense Development (ADD), Yuseong P.O. Box 35-5, Daejeon 34602, Korea
(*Received 13 December 2018 • accepted 25 May 2019*)

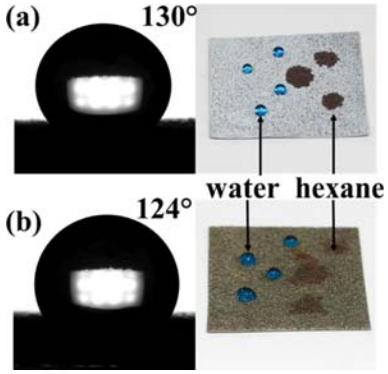

Fig. S1. Contact angles and images of (a) Nickel foam coated with PVDF+20 wt% Silica nanoparticles (b) Nickel foam coated with PVDF only.